

Spectral Evolution of PKS 2155-304 observed with *BeppoSAX* during an Active Gamma-ray Phase

L.Chiappetti ¹, L.Maraschi ², F.Tavecchio ^{2,1}, A.Celotti ³, G.Fossati ³, G.Ghisellini ²,
P.Giommi ⁴, E.Pian ⁵, G.Tagliaferri ², A.Treves ⁶, C.M. Urry ⁷, Y.H. Zhang ³

Received _____; accepted _____

Submitted to ApJ 19/11/1998 Revised 11/03/1999 Accepted 19/03/1999

¹Istituto di Fisica Cosmica G.Occhialini, IFCTR/CNR, Milano, Italy

²Osservatorio Astronomico di Brera, Milano and Merate, Italy

³International School of Advanced Studies, SISSA/ISAS, Trieste, Italy

⁴BeppoSAX Science Data Centre, SDC/ASI, Rome, Italy

⁵Istituto ITESRE, CNR, Bologna, Italy

⁶Istituto di Fisica, Università dell'Insubria, Como, Italy

⁷Space Telescope Science Institute, Baltimore MD, USA

ABSTRACT

We present the results of *BeppoSAX* observations of PKS 2155–304 during an intense γ -ray flare. The source was in a high X-ray state. A temporal analysis of the data reveals a tendency of the amplitude of variations to increase with energy, and the presence of a soft lag with a timescale of the order 10^3 s. A curved continuum spectrum, with no evidence of spectral features, extends up to ~ 50 keV, while there is indication of a flatter component emerging at higher energies, consistent with the interpretation of the broad band spectral energy distribution (SED) as due to synchrotron self-Compton (SSC) emission from a single region. Notably, the fitting of the SED with such a model is consistent with an interpretation of the detected soft lag as due to radiative cooling, supporting the idea that radiation losses play an important role in variability. The observed shifts of the SED peaks between the lowest and highest flux levels can be accounted for by an increase of the “break” energy in the relativistic particle spectrum. The model predicts emission at TeV energies in good agreement with the recently reported detection.

Subject headings: BL Lacertae objects: individual (PKS 2155-304) — X-rays: galaxies

1. Introduction

BL Lacertae objects are a rare class of Active Galactic Nuclei, characterized by strong and variable non-thermal emission, extending from the radio to the gamma-ray band. The non-thermal continuum is commonly attributed to synchrotron and inverse Compton (IC) radiation emitted in a relativistic jet pointing towards the observer (e.g. Urry & Padovani 1995).

PKS 2155-304 is one of the brightest BL Lac in the X-ray band and one of the few detected in γ -rays by the EGRET experiment on CGRO (Vestrand, Stacy & Sreekumar 1995). Its broad band spectrum indicates that the radio to X-ray emission is due to synchrotron radiation with a peak in the power per decade distribution between the UV and the soft X-ray band, corresponding to the definition of an High Frequency Peak BL Lac (HBL) (Padovani & Giommi 1995). The gamma-ray spectrum in the EGRET range (0.1–10 GeV) is flat ($\alpha_\gamma \simeq 0.7$) indicating that the peak of the inverse Compton power is beyond ~ 10 GeV. The source has only recently been detected in the TeV band (see below).

In the past years PKS 2155-304 has been the target of numerous multiwavelength campaigns involving observations from the X-rays to longer wavelengths. In the May 1994 campaign (Urry et al. 1997) a well defined flare was seen in the X-ray band (ASCA), followed by less pronounced flares in the EUVE and UV ranges, lagging the X-rays by one and two days, respectively. A time lag between variations in different X-ray bands (0.5-1 and 2.2-8 keV) was also reported (Makino et al. 1996). In a previous multiwavelength campaign, based on ROSAT and IUE, correlated low amplitude fluctuations were observed but no lag larger than a few hours was seen between the X-ray and UV variations (Edelson et al. 1995).

According to the basic scenario the X-ray emission is due to synchrotron radiation from the highest energy electrons and the complex spectral variability observed in this band

therefore reflects the injection and radiative evolution of freshly accelerated particles.

No observations at other wavelengths simultaneous with one in gamma-rays were ever obtained previously for this source, yet it is essential to measure the IC and synchrotron peaks at the same time, in order to unambiguously constrain emission models (e.g Dermer, Sturmer & Schlickeiser 1997; Tavecchio Maraschi & Ghisellini 1998).

For this reason, having been informed by the EGRET team of their observing plan and of the positive results of the first days of the CGRO observation, we decided – with the agreement of the *BeppoSAX* TAC and the collaboration of the *BeppoSAX* SDC – to swap a pre-scheduled target of our *BeppoSAX* blazar program with PKS 2155-304. During November 11-17 1997 (Sreekumar & Vestrand 1997) the γ -ray flux from PKS 2155-304 was very high, roughly a factor of three greater than the highest flux previously measured from this object. *BeppoSAX* pointed at this source for about 1.5 days starting November 22. A quick-look analysis indicated that also the X-ray flux was close to the highest detected level (Chiappetti & Torroni 1997) and higher by a factor two than that observed by *BeppoSAX* in 1996 (Giommi et al. 1998). During the completion of this work we have been informed that the source was detected at TeV energies by the University of Durham TeV telescope Mark 6 (Chadwick et al. 1998) at the time of the *BeppoSAX* observations.

Here we report and discuss the data obtained by *BeppoSAX*. The structure of the paper is as follows: the relevant information on the observations is given in section 2 and the data analysis methods are presented in detail for each instrument in section 3; light curves and temporal analysis are reported in section 4, while the spectral results are the subject of section 5. Finally, in section 6 the implications for theoretical models are discussed. Conclusions are summarized in Section 7.

2. Observations

The *BeppoSAX* scientific payload (see Boella et al. 1997a) includes four Narrow Field Instruments (NFIs) pointing in the same direction. Namely, there are two imaging instruments : the Low Energy Concentrator Spectrometer (LECS), sensitive in the range 0.1–10 keV (Parmar et al. 1997), and the Medium Energy Concentrator Spectrometer (MECS), sensitive in the range 1.3-10 keV (Boella et al. 1997b) and consisting of three identical units. Both the LECS detector and the three MECS detectors are Gas Scintillation Proportional Counters (GSPC) and are in the focus of four identical X-ray telescopes. Additionally there are two collimated instruments: the High Pressure Gas Scintillation Proportional Counter (HPGSPC), sensitive in the 4-120 keV range (Manzo et al. 1997) and the Phoswich Detector System (PDS), sensitive from 12 to 300 keV (Frontera et al. 1997).

BeppoSAX NFIs observed PKS 2155-304 for slightly less than 1.5 days from 16:03 UT of November 22 to 01:35 UT of November 24 1997. The total exposure time was of about 22 ks for the LECS and 63 ks for the two MECS units now in operation (M2 and M3), with an average count rate of 0.64 (1.8-10 keV) cts/s in a single MECS unit (corresponding to about 5 mCrab) and 2.21 cts/s in the LECS (0.1-4 keV band).

The HPGSPC and PDS were operated in the customary collimator rocking mode, where each collimator points alternately at the source and at the background for 96 s. In the case of the HPGSPC there is a single collimator, so the whole instrument is looking at the target for half of the time, and in the offset negative direction for the other half. The resulting source exposure time was 29 ks and the source was detected at least up to 30 keV with a rate of 0.5 cts/s. The PDS has two collimators: at any time one of them looks at the source, and the other one at the background. Therefore the target is observed continuously (in our case the exposure time was 28+29= 57 ks) but using only half of the collecting area, with a count rate between 0.2 and 0.3 cts/s.

3. Data Reduction

The data reduction for MECS, PDS and HPGSPC was done using the XAS software (Chiappetti & Dal Fiume 1997) on telemetry files contained in the Final Observation Tapes. For the LECS we have used the linearized, cleaned event files version rev.1.0 generated at the *BeppoSAX* Science Data Centre (SDC).

We have preliminarily selected the intervals in which the satellite was pointing at the source (unocculted by the Earth, i.e. Earth elevation angle greater than 3 degrees) using the information in the attitude files. In addition, for collimated instruments, we have excluded the first 5 minutes after egress from the South Atlantic Geomagnetic Anomaly, when the instrument gain is being calibrated.

3.1. Imaging instruments

As part of the standard data accumulation for both LECS and MECS, a number of corrections is applied to each photon, namely the positional coordinates are linearized (correcting for geometrical distortion), the energy of each photon is referred to the detector centre (compensating for known spatial disuniformities of gain) and corrected to a standard gain using the gain histories to remove the temperature dependency of gain. In our case we verified the stability of the gain within at worst 2% during the initial orbits.

For both instruments the preferred background subtraction method is to use a background spectrum accumulated from blank field exposures in the *same* detector region where the target spectrum is accumulated. The accumulation of a simultaneous background spectrum in a *surrounding* annulus would instead include a residual contribution from the target. In fact, an extraction radius of the order of 8 arcmin, as used here, leaves out ~ 2 -4% of the PSF, depending on energy.

3.1.1. *MECS*

Source spectra and light curves were accumulated in a circular region of 8.4 arcmin radius around the target position. In order to improve particle background rejection, we also applied Burst Length thresholds (channel 25-55 for M2 and 27-60 for M3) consistent with the standard response matrices.

The background was accumulated in the same region from a large dataset of blank fields obtained during the *BeppoSAX* Performance Verification (PV) phase (and available to IFCTR as a *BeppoSAX* hardware institute) for a total exposure time of 1120 ks. In addition to the considerations made above, in the case of the MECS this has to be preferred also because the outermost part of the field of view is known to be affected by residual contamination from misplaced calibration events (Chiappetti et al. 1998).

3.1.2. *LECS*

The LECS data analysis was based on the cleaned and linearized event files processed at the SDC. The events were extracted with XSELECT within a circle centered on the source of radius of 8.5 arcmin. Since the count rate of the source is very high, the background is not very important and we used the standard background files supplied by SDC. The spectral analysis was performed using the calibrations released in September 1997.

3.2. Collimated instruments

3.2.1. *PDS*

The standard PDS spectra accumulation occurs via the following procedure. One first creates the time profiles of both collimator positions (sampled at 1 s resolution),

and generates for each three sets of time windows, corresponding to stable positions on source and offset in the positive (off+) and negative (off-) directions. Then three spectra in raw PHA channels for each unit are accumulated over the respective time windows (background+source, and background in the off+ and off- cases).

A merged background spectrum for each unit (exposure-weighted sum of the off+ and off- spectra) is then generated and subtracted from the on source spectrum. In order to sum the net spectra of the four units, one has to equalize the respective gain (i.e. convert from PHA channels to keV using unit-specific relations assuming a standard gain), which is done contextually with a user-selected rebinning (usually logarithmic) in energy space.

During accumulation one also applies default rise time (RT) threshold (channels 3-150) to improve rejection of non-X-ray events. For medium-weak sources one can apply an additional set of narrower energy-dependent RT thresholds (so called “PSA correction” method). The RT of individual photons is compensated for temperature variations with respect to the nominal temperature for which the thresholds have been generated. In this way a 40 % reduction of the background is achieved (from 10 to 6 cts/s), with a smaller effect on the net rate (which is accounted for by a 10-20 % adjustment of the cross normalization of the PDS response matrix with respect to the MECS one): in our case we obtain on the overall energy range 0.27 ± 0.05 cts/s (no correction) and 0.21 ± 0.03 cts/s (with correction), which are consistent within the errors.

We verified the quality of the background subtraction, by subtracting the off+ and off- raw background spectra of each unit from each other, and then summing the difference spectra of the four units exactly in the same way described above for the production of net spectra. Indeed the resulting signal (0.06 ± 0.06 cts/s) is consistent with zero.

PDS data may be affected by spurious spikes, due to the *fluctuations* of meta-stable phosphorescence induced in the crystals by particles, interpreted by the electronics as spikes

in the count rate (as high as 300 cts in a 0.1 s interval). A spike filtering has been applied to all spectra and light curves, rejecting all time intervals where the scientific data rate (in the PHA range 10-350 and in the RT range 3-130) are above 25 cts/s.

Since the signal is weak, we have not attempted to accumulate binned light curves. Similarly to MECS and HPGSPC, we used instead large bins of variable size (of the order of 1 hr or less) corresponding to unocculted intervals in each orbit, we accumulated three separate light curves for each PDS unit (for the on source, off+ and off- cases, taking in due account the exposure fraction of each bin), made a weighted combination of the off+ and off- curves, subtracted it from the source+background one, and finally summed the four unit net curves.

3.2.2. *HPGSPC*

The standard HPGSPC spectra accumulation is similar to the procedure described above for the PDS. However one has only one collimator position time profile and just two disjoint time windows, corresponding to stable positions on source and offset in the negative directions. Then one accumulates two spectra over the respective time windows (background+source, and offset background), also applying the Burst Length thresholds (channels 80-115) to improve rejection of non-X-ray events. The background has to be corrected before subtraction. by adding a difference spectrum which compensates for effects due to the different position of the collimators (mainly the illumination by the calibration sources).

As for the PDS, we used “coarse variable bins”, as defined above, to generate light curves for the on source and offset cases. We subtracted the uncorrected background plus a further constant, corresponding to the integral of the difference spectrum in the wished

PHA channel range. We intended to “hook up” our HPGSPC data with MECS and PDS data in the overlapping energy ranges. However the HPGSPC 5-10 keV curve shows excesses with respect to the MECS in a couple of orbits, related to ^{55}Fe calibration events not rejected properly by the onboard tagging. Further occasional deviations still present in the 7-10 keV range suggest that the stability of the difference spectra with time is poorly known, throwing doubts also on the confidence of HPGSPC 10-16 keV light curves.

4. Results

4.1. Light curves

In Fig. 1 we show the MECS light curve at 120 sec resolution. Epochs of high, low and intermediate intensity, which will be used to integrate spectra at different intensity levels, are indicated with letters A-F (see Section 4.2). In Fig. 2 (top panels) we show the light curves binned over 1000 s in different energy bands: 0.1-2 keV for the LECS, 2-4 keV and 4-10 keV for the MECS. The source reaches a peak after the first 2 hours of observation (indicated as A in Fig. 1) and declines by a factor 3 (max/min) in the following 10 hours. A smaller flare (indicated as D) follows and the light curve seems to stabilize in the interval indicated as F. The variability timescale appears to be well resolved and no episode of very fast variability ($Fdt/dF < 1h$) is apparent.

The most rapid variation observed (the decline from the peak at the start of the observation) has a halving timescale of about 2×10^4 s, similar to previous occasions (see e.g. Urry et al. 1997). Light curves from the higher energy instruments were derived as detailed in section 2, but no significant variability was detected due to poor statistics.

The variability amplitude is different in the three bands, increasing with increasing energy. In order to better characterize this energy dependence, hardness ratios between the

2-4/0.1-2 keV (HR1) and the 4-10/2-4 keV bands (HR2) were computed. They are shown in the last panels of Fig. 2 (lower panels). HR1 has smaller uncertainties and clearly increases with intensity in a correlated fashion on the timescale of each peak. However the correlation is not biunivocal: HR1 has the same value at the first two peaks (A and D), which have significantly different intensities, and is lower towards the end of the observation, when the average intensity is similar to that of peak D. Note also that for both the first and the second peak the hardness ratio is high already before the peak is reached. HR2 does not show a clear trend, which could be due to the larger uncertainties and to the smaller energy range. The issue of spectral variability is further discussed below (sect. 4.2.3).

We looked for time lags between variations at different energies as suggested by the ASCA observations of this same source and of Mrk 421 (Makino et al. 1996, Takahashi et al. 1996). The presence of a soft lag is indicated by the fact that the hardness ratio increases *before* the intensity peaks, as it is the case in our light curve.

To quantify the lag we used the Discrete Correlation Function (DCF) method developed by Edelson & Krolik (1988) for data sets with irregular spacings. We binned the light curves in smaller and smaller bins since no lag was apparent for bin sizes larger than 1000 s. In Fig. 3 we show the DCF obtained correlating the light curves in the bands 0.1-1.5 (LECS) and 3.5-10 keV (MECS). A gaussian fit, which takes into account the overall symmetry of the distribution around the peak, yields a maximum corresponding to a soft lag of 0.50 hr (with a 1σ error of 0.08 hr). We also applied the Minimum Mean Deviation (MMD) method (Hufnagel & Bregman 1992) (Fig. 4). Here the correlation estimator is the mean deviation of the two cross correlated light curves: the minimum mean deviation corresponds to the best cross correlation. A gaussian fit to this minimum gives again a soft lag of 0.33 ± 0.07 hr.

The issue of the lags and their uncertainties, estimated with a Monte Carlo procedure,

is discussed in detail in Treves et al. (1998) and Zhang et al. (1999), where a comparison is made with the 1996 *BeppoSAX* (Giommi et al. 1998) and 1994 ASCA data (Makino et al. 1996)

4.2. Spectra

We analyzed first the overall spectrum from the entire observation separately for each instrument and then combining different instruments. We also studied spectral variability, accumulating spectra in the time intervals indicated as A to F in Fig. 1. When not differently stated we used in the fits the value of the galactic column density reported by Lockman & Savage (1995), $N_H = 1.36 \times 10^{20} \text{ cm}^{-2}$.

For the spectral fitting procedures the LECS and MECS data were binned in energy according to the template provided by SDC (Fiore & Guainazzi 1997) which takes into account the effective energy resolution of the spectrometers. For the high energy instrument data have been severely rebinned as described below. In all cases we considered for the LECS the energy range 0.1-4 keV, for the MECS 2-10 keV.

The response matrices are generated according to the accumulation conditions (extraction radius, binning etc.) for the MECS and PDS case using the latest version of the XAS software, while for LECS and HPGSPC case standard matrices are used, as released in September 1997 (with optional rebinning). Results of the fits are summarized in Table 1.

4.2.1. Single Instruments

LECS A single power law is a poor fit to the LECS data, although it yields an N_H value quite close to the galactic one. An acceptable fit is obtained by modelling the spectrum

with a broken power law (see Table 1); in the latter case too the N_H determined by the fit is consistent with the galactic one, which was therefore fixed in all the following fits. The residuals of this fit do not show clear evidence of spectral features in absorption or emission. In particular we do not detect absorption near 0.6 keV as seen in some previous observations (Canizares & Kruper 1984; Madejski et al. 1991; see however Brinkmann et al. 1994).

MECS The MECS alone is not sensitive to low values of N_H because of the low energy cutoff induced by the Beryllium window. A fit with a single power law and free column density gives χ^2 close to unity, but yields an ill-determined N_H of several 10^{21} cm⁻², inconsistent with the results from the LECS. When fixing N_H to the galactic value, a broken power law model describes well the spectrum within the 2-10 keV band (see Table 1). Note that the spectral index in the higher energy range of the LECS (1-4 keV) is similar to that in the lower energy range of the MECS (2-3 keV) giving us confidence that the increasing slope suggested by the fits is a good representation of the spectrum.

HPGSPC The HPGSPC data were rebinned “ad hoc” into 8 bins. The signal is present very clearly ($> 4\sigma$) up to 13 keV and with a lower statistical significance up to at least 24 keV (i.e. below the Xe K edge). As MECS and HPGSPC are very well cross-calibrated (Cusumano et al. 1998) and since this spectrum lies well on the extrapolation of the MECS fit, it has been fitted only in combination with spectra from other instruments.

PDS For the PDS we used a very coarse grouping in just 4 logarithmic bins. The signal from the source is clearly visible in the first bin (up to 26 keV), and remains present at a non-zero level (although with a poorer significance, $\simeq 2\sigma$) in the other bins. Fitting the PDS data with a single power law yields a poor result, with a spectral index *flatter* than in

the MECS band.

4.2.2. Combined Spectra

We fitted the composite LECS+MECS spectrum over the entire range 0.1-10.5 keV (see Table 1). Given that the single instrument spectra are well described by broken power law models, we tried to reproduce the composite spectrum with the same model. We allowed for a free relative normalization between the LECS and MECS data and the best fit value found (LECS norm/ MECS norm $\simeq 0.7$) is consistent with previous works. However the fit is unacceptable. In Fig. 5 we show the results of the fitting procedure : the model does not represent the data well ($\chi^2_{red} = 2.3$) and the shape of the residuals indicates that the spectrum is flatter than the model at the lowest energies and steeper at the highest ones. Thus a model describing a more continuous steepening is required, in agreement with the results of the fits to individual spectra which yield at least two “break” energies (at ~ 1.2 and ~ 3.2 keV respectively) with spectral indices $\Gamma \sim 2.1, 2.6$ and 2.9 . This trend was also found (for this same source) by Giommi et al. (1998), who indeed showed that a good fit can be obtained using a curved model.

Fitting together the MECS and PDS data yields spectral parameters very similar to those obtained for the MECS alone. A cross normalization of 0.8 was used. The residuals show that the PDS data are consistent with an extrapolation of the MECS fit up to about 50 keV. Above this energy the PDS data present a marginal hint of an excess suggesting - as already found for the PDS alone - a flattening of the spectrum.

Adding also the HPGSPC spectrum to the dataset, and fitting all three instruments gives again results similar to those obtained for the MECS alone (Fig. 6). Additionally, if one uses MECS data above the 3.2 keV break together with HPGSPC data, they are

compatible ($\chi^2 = 55$ for 49 DoF) with a broken power law model with the first spectral index Γ_1 fixed to the value ~ 2.9 derived from the MECS fit, a break around 10 keV and a flatter slope $\Gamma_2 \sim 2.2$ (no formal simultaneous fit of the break energy and Γ_2 is possible). This is a further element in favour of a flattening of the spectrum at high energies.

4.2.3. Spectral variability

In view of a discussion on spectral variability the overall observation period has been divided into smaller intervals (indicated as A to F in Fig. 1) using the following approximate intensity windows (referred to a single MECS unit): peak, above 0.8 cts/s (interval A); intermediate (intervals B, D and F); dip, below 0.5 cts/s (intervals C and E). We have then accumulated spectra with the standard prescriptions described above for each interval, and also for the combinations B+D+F and C+E. Additionally, we have divided interval D into two parts (“rise” and “fall”) and taken the ratio of the relevant spectra, which has been found to be consistent with unity.

In order to have a model independent description of the spectral variability we have computed the spectral ratio between the flaring (A) and the lowest states (C and E). The result is plotted in Fig. 7 : the ratio continuously increases with energy, yielding clear evidence that the flaring state is harder than the low state. Since this ratio varies by a factor of about 2 over two decades the associated change in spectral index can be estimated as only $\Delta\alpha \simeq 0.15$.

Both the LECS and MECS spectra for the high, intermediate and low states were separately fitted with broken power laws, fixing the value of Γ_1 for the MECS fit at the value of Γ_2 obtained from the LECS. The results are reported in Table 1. They are consistent with a hardening of the spectrum with increasing intensity, but the magnitude of this

variation is small, as estimated above, comparable with the errors in the fit parameters.

5. Broad Band Spectral Energy Distributions

In order to estimate the physical parameters of the emitting region we constructed broad band spectral energy distributions (SED) based on the deconvolved LECS and MECS *BeppoSAX* data at *maximum* and *minimum* intensity during the present observation (Fig. 8). At higher energies, the PDS data represent averages over the whole *BeppoSAX* observation period. At γ -ray energies the EGRET spectrum is plotted as from the discovery observation (Vestrand, Stacy & Sreekumar 1995) and also with an intensity multiplied by a factor three, to represent the gamma-ray state of 11-17 November 1997, as communicated by Sreekumar & Vestrand (1997). The *BeppoSAX* observation occurred near the end of the two-week CGRO observation while the high gamma-ray state was recorded during the first days. In the absence of a gamma-ray flux exactly simultaneous with the *BeppoSAX* data we consider the two sets of gamma-ray intensities as encompassing the actual values.

At UV wavelengths we plot the maximum and minimum fluxes observed with IUE (Edelson et al. 1992, Urry et al. 1993, Pian et al. 1997) and at other wavelengths the maxima and minima as observed during the 1991 and 1994 multiwavelength campaigns (Courvoisier et al. 1995, Pesce et al. 1997).

The shape of the SED can be interpreted as due to two components: the first one, peaking in the soft X-ray range, is commonly attributed to synchrotron radiation while the second, peaking above 10 GeV as suggested by the flat γ -ray spectrum, can be accounted for by inverse Compton scattering of the synchrotron photons off the high energy electrons that produced them, namely the Synchrotron Self-Compton process (SSC) (e.g. Ulrich, Maraschi & Urry 1997 and references therein).

A simple version of this model considers emission from a homogeneous spherical region of radius R , whose motion can be characterized by a Doppler factor δ , filled with a magnetic field B and with relativistic particles whose energy distribution is described by a broken power law (the latter corresponds to 4 parameters: two indices n_1 , n_2 , a break energy $\gamma_b mc^2$ and K , a normalization constant). As discussed in detail by Tavecchio, Maraschi & Ghisellini (1998) the seven model parameters listed above can be strongly constrained by using seven observational quantities, namely the two spectral slopes (in the X- and γ -ray bands), the frequency and flux of the synchrotron peak, a flux value for the inverse Compton component emission and a lower limit to the IC peak frequency. Assuming $R = ct_{var}$ with a variability timescale $t_{var} = 2$ hr, the system is practically closed and we obtain *univocally* a set of physical parameters for the source, with uncertainties depending on those of the observed quantities involved.

Fig.4 of Tavecchio, Maraschi & Ghisellini (1998) shows the allowed region in the $B - \delta$ space derived for PKS 2155-304 with values of the observational quantities encompassing those derived here. A lower limit $\delta > 15$ is set by the "internal" transparency condition for TeV γ -rays, while the limits derived from the modeling of the SED fall somewhat above this.

In Fig. 8 we show two SEDs computed with the SSC models described above aimed at reproducing the high and low X-ray states observed with *BeppoSAX*. We (arbitrarily) assumed that the lower intensity X-ray state corresponds to the gamma-ray emission reported in 1995. The parameters of the model for the lower state have the following values: $\delta = 18$, $B=1$ G, $R = 3 \times 10^{15}$ cm, $n_1 = 2$, $n_2 = 4.85$, $K = 10^{4.7}$, $\gamma_b = 10^{4.5}$. The inverse Compton emission is computed here with the usual step approximation for the Klein-Nishina cross section, i.e. $\sigma = \sigma_T$ for $\gamma\nu_t < mc^2/h$ and $\sigma = 0$ otherwise, where γ is the Lorentz factor of the electron and ν_t is the frequency of the target photon.

The comparison of the flaring spectrum with the lower intensity one in Fig. 8 shows

that the *peak* in the SED shifted to higher energies during the flare. In fact the peak occurs at about 1 keV during the flare, while in the fainter states it falls towards the lower end of the *BeppoSAX* range ($\simeq 0.2$ keV). A similar behavior was observed in Mrk 421 with ASCA (Takahashi et al. 1996) and with *BeppoSAX* (Fossati et al. 1998). A much more extreme case occurred in Mrk 501, when in a state of exceptional activity the SED peak was observed to be in the 100 keV range (Pian et al. 1998).

Therefore, in the model for the flaring state, the break energy of the electron spectrum was shifted to higher energies ($K = 10^{4.8}$, $\gamma_b = 10^{4.65}$) leaving the other parameters unchanged. Correspondingly also the IC peak increased in flux and moved to higher energies. Both effects are however reduced with respect to the “quadratic” relation expected in the Thomson limit since for the required very high energy electrons the suppression due to the Klein-Nishina regime plays an important role.

The models predict TeV emission at a detectable level. Indeed, towards the completion of this work, we have been informed of the detection of high energy γ -rays by the Mark 6 telescope (Chadwick et al. 1998). Part of the Mark 6 observing period overlaps with that of *BeppoSAX* and EGRET. Although the exact flux level simultaneous to the *BeppoSAX* one has not been reported, in November 1997 the source was seen by the Mark 6 telescope at its highest flux (Chadwick et al. 1998). The time averaged flux corresponds to 4.2×10^{-11} ph cm $^{-2}$ s $^{-1}$ above 300 GeV (and extending up to > 3 TeV).

Indeed the model for the lower intensity state reproduces the average TeV emission flux level remarkably well. A more detailed test, comparing the TeV fluxes associated with different X-ray states will be hopefully possible with future observations.

Current models of the IR background (Malkan & Stecker 1998) predict an optical depth between 1 and 2 for 1 TeV photon from a source located at $z \sim 1$ (Stecker & de Jager 1998). The resulting flux reduction would be still consistent with our model. Signatures of

this effect may be found in the future from a measurement of the TeV spectral shape.

Note that, given the flat soft X-ray spectrum, it would be impossible to reproduce with these same models also the non-simultaneous optical-UV data reported in the figure. Since the variations occur on longer time scales in the lower energy bands, the optical-UV flux may derive from a larger spatial region which acts as a reservoir for the partially cooled particles. At higher energies instead we may observe the radiation from the freshly accelerated particles, before they can accumulate in the reservoir. In this case, a single homogeneous region is not sufficient to describe the full broad band SED. Alternatively a more complex spectral shape for the electron energy distribution has to be assumed.

6. Spectral Dynamics

The time resolved continuum spectroscopy, made possible by sensitive and broad band instruments like ASCA and *BeppoSAX*, has triggered the need for time dependent models describing the changes in particle spectra due to acceleration, energy losses and diffusion. The problem is in general complex and only some simplified cases have been treated up to now (e.g. Kirk, Rieger & Mastichiadis 1998, Dermer 1998, Makino 1998). In addition, light travel time effects through the emitting region may be important (Chiaberge & Ghisellini 1998).

A crucial point in this problem is the measurement and interpretation of lags of the soft photons with respect to the harder ones. These can be produced through radiative cooling if the population of injected (accelerated) electrons has a low energy cut off or possibly a sharp low energy break, as clearly shown by Kazanas, Titarchuk & Hua (1998). If so, the observed lag τ_{obs} depends only on the value of the magnetic field (assuming synchrotron losses are dominant, as is roughly the case for this source) and δ . Their relation can be

expressed as

$$B\delta^{1/3} \simeq 300 \left(\frac{1+z}{\nu_1} \right)^{1/3} \left[\frac{1 - (\nu_1/\nu_0)^{1/2}}{\tau_{obs}} \right]^{2/3} G \quad (1)$$

where ν_1 and ν_0 represent the frequencies (in units of 10^{17} Hz) at which the observed lag (in sec) has been measured.

It is interesting to note that the value of the lag (0.5 hrs) inferred from the present *BeppoSAX* observations yield a B and δ combination consistent with the parameters obtained *independently* from the spectral fitting. This argument supports the radiative interpretation of the observed X-ray variability. An alternative possibility recently put forward by Dermer (1998) is that the flare decay is due to deceleration of the emitting plasma by entrainment of external matter as proposed for γ -ray bursts. A detailed model would be needed for a quantitative comparison with the present data.

We recall that also in Mrk 421, a source closely similar to PKS 2155-304 in the SED, similar values of the lag have been found (Takahashi et al. 1996). In fact the same arguments applied here to PKS 2155-304 give similar estimate of the physical parameters for Mrk 421 (see Tavecchio Maraschi & Ghisellini 1998). In the case of the other well established TeV source Mrk 501 lags have not been measured up to now.

7. Summary and Conclusions

Simultaneous multiwavelength monitoring has proved to be a very powerful tool to test and constrain emission models for blazars. The *BeppoSAX* observations of PKS 2155-304 here reported, were partially overlapping with an intense γ -ray flare detected by EGRET and with observations at TeV energies by the Mark 6 telescope which also revealed a high flux.

Although exactly simultaneous γ -ray data are not available at the time of writing, the X-ray data alone already provide us with interesting results. The X-ray flux was almost at the highest level ever detected. A curved spectral component, which can be identified with the high energy end of the synchrotron emission, extends up to about 50 keV, while at higher energies the spectrum flattens, plausibly revealing the contribution of inverse Compton emission.

Indeed this is what is generally expected in the context of emission from a relativistic jet, which seems quite convincingly to account for the SED of blazars. Within the blazar class, the synchrotron and inverse Compton components of low power BL Lac objects, as is the case for PKS 2155–304, tend to peak at the highest energies (X-ray and TeV energies, respectively) and the synchrotron photons probably dominate the seed radiation field to be upscattered to γ -ray energies.

Further constraints on the structure and physical parameters of the emitting source come from adding to the spectral the temporal information. Indeed we find that SSC emission from a homogeneous region can consistently account for both the broad band SED and the soft lag detected by *BeppoSAX*, the latter being due to radiative cooling of the high energy part of the electron distribution.

An interesting and testable prediction of this interpretation is the emission of TeV photons, which indeed has been found *a posteriori* to be in remarkably good agreement with the results recently reported by the Mark 6 team (Chadwick et al. 1998).

We thank L.Piro, *BeppoSAX* Mission Scientist, and the (chairman and members of) *BeppoSAX* Time Allocation Committee for allowing us to perform this observation in replacement of another target allocated to us, and the Mission Planning team at *BeppoSAX* SDC for the prompt scheduling. We also gratefully acknowledge conversations

with D.Dal Fiume for extremely useful hints on PDS data reduction, and some suggestions by A.Santangelo about HPGSPC data reduction. AC and GF thank the Italian MURST for financial support.

Table 1. Best fit parameters

Data Set	N_H ^a	Γ ^b	χ^2/DoF ^b	Γ_1 ^c	Γ_2 ^c	E_b (keV) ^c	χ^2/DoF ^c	Flux ^d
LECS, all	$2.1_{-0.05}^{+0.1}$	2.38 ± 0.02	207/48
	1.4 ± 0.1	2.09 ± 0.05	2.54 ± 0.04	1.1 ± 0.1	56.4/45	...
	1.36 (fix)	2.21 ± 0.01	57.4/48	2.06 ± 0.02	2.54 ± 0.04	1.1 ± 0.1	57.4/47	...
MECS, all	41 ± 20	2.92 ± 0.04	74.1/56
	1.36 (fix)	2.78 ± 0.02	118/57	$2.64_{-0.08}^{+0.06}$	$2.88_{-0.03}^{+0.07}$	3.2 ± 0.1	76.2/55	...
PDS,all	...	$2.1_{-0.8}^{+1.7}$	5.0/2
LECS+MECS, all	1.36 (fix)	2.09 ± 0.02	2.76 ± 0.02	1.4 ± 0.1	244.0/105	...
MECS+PDS, all	1.36 (fix)	$2.65_{-0.09}^{+0.05}$	2.90 ± 0.05	3.2 ± 0.1	87.2/58	...
MECS+HPGSPC+PDS, all	1.36 (fix)	$2.65_{-0.08}^{+0.05}$	2.89 ± 0.04	3.2 ± 0.1	85.8/64	...
LECS+MECS								
all	1.36 (fix)	2.07 ± 0.02	2.63 ± 0.03	1.2 ± 0.1	153.4/103	0.81
				2.63 (fix)	2.90 ± 0.04	3.3 ± 0.2		
A	1.36 (fix)	2.00 ± 0.04	2.57 ± 0.07	1.2 ± 0.2	145.3/102	1.27
				2.57 (fix)	2.97 ± 0.12	3.5 ± 0.5		
B+D+F	1.36 (fix)	2.08 ± 0.02	2.66 ± 0.03	1.2 ± 0.1	130.8/103	0.85
				2.66 (fix)	2.90 ± 0.05	3.2 ± 0.3		
C+E	1.36 (fix)	2.15 ± 0.05	2.61 ± 0.09	1.1 ± 0.1	92.7/102	0.54
				2.61 (fix)	2.89 ± 0.07	2.9 ± 0.2		

^a 10^{20} cm^{-2}

^bsingle power law model

^cbroken power law model

^dFlux at the source in the 2-10 keV band, in $10^{-10} \text{ erg cm}^{-2} \text{ s}^{-1}$

^eAll errors quoted are at 90 % confidence level

REFERENCES

- Boella, G., Butler, R. C., Perola, G. C., Piro, L., Scarsi, L., & Bleeker, J. A. M. 1997a, A&AS, 122, 299
- Boella, G., et al. 1997b, A&AS, 122, 327.
- Brinkmann, W., et al. 1994, A&A, 288, 433
- Canizares, C. R. & Kruper, J. 1984, ApJ, 278, L99
- Chadwick, P.M., et al. 1998, ApJ, accepted (astro-ph/9810209)
- Chiaberge, M. & Ghisellini, G., 1998, MNRAS, submitted (astro-ph/9810263)
- Chiappetti, L. & Torroni, V. 1997, IAU Circ., 6776, 2
- Chiappetti, L. & Dal Fiume D. 1997, Proc. of the 5th Workshop “Data Analysis in Astronomy” Erice 27 October - 3 November 1996, Ed. V. Di Gesù et al., pag. 101.
- Chiappetti, L., Cusumano, G., Del Sordo, S., Maccarone, M.C, Mineo, T. & Molendi S. 1998, Nucl. Phys. B Proc. Suppl., 69, 610
- Courvoisier, T. J.-L., et al. 1995, ApJ, 438, 108
- Cusumano, G., et al. 1998, Intercalibration of the *BeppoSAX* Narrow Field Instruments with Crab Nebula, in preparation
- Dermer, C. D., Sturmer, S. J., & Schlickeiser, R. 1997, ApJS, 109, 103
- Dermer, C. D. 1998, ApJ, 501, L157
- Edelson, R., Pike, G. F., Saken, J. M., Kinney, A., & Shull, J. M. 1992, ApJS, 83, 1
- Edelson, R., et al. 1995, ApJ, 438, 120

- Edelson, R. A. & Krolik, J. H. 1988, *ApJ*, 333, 646
- Fiore, F., & Guainazzi, M., 1997, *SAX Scientific Analysis Cookbook : Spectral Analysis*,
<http://www.sdc.asi.it/software/cookbook/spectral.html>
- Fossati, G. et al. 1998, *Nucl. Phys. B Proc. Suppl.*, 69, 423
- Frontera, F., Costa, E., Dal Fiume, D., Feroci, M., Nicastro, L., Orlandini, M., Palazzi, E.,
& Zavattini, G. 1997, *A&AS*, 122, 357
- Giommi, P., et al. 1998, *A&A*, 333, L5
- Hufnagel, B. R. & Bregman, J. N. 1992, *ApJ*, 386, 473
- Lockman, F. J. & Savage, B. D. 1995, *ApJS*, 97, 1
- Kazanas, D., Titarchuk, L. G., & Hua, X.-M. 1998, *ApJ*, 493, 708
- Kirk, J. G., Rieger, F. M., & Mastichiadis, A. 1998, *A&A*, 333, 452
- Madejski, G. M., Mushotzky, R. F., Weaver, K. A., Arnaud, K. A., & Urry, C. M. 1991,
ApJ, 370, 198
- Malkan, M. A. & Stecker, F. W. 1998, *ApJ*, 496, 13
- Manzo, G., Giarrusso, S., Santangelo, A., Ciralli, F., Fazio, G., Piraino, S., & Segreto, A.
1997, *A&AS*, 122, 341
- Makino, F., et al. 1996, *Röntgenstrahlung from The Universe*, Ed. Zimmermann, H.U.,
Trumper, J.E., Yorke, H., MPE Report 263, pag. 413
- Makino, F. 1998, *Proc. of the BL Lac Phenomenon meeting*, Turku, Finland, 22-26 June
1998, Edited by L.O.Takalo, *PASP Conf. Series* in the press.
- Padovani, P. & Giommi, P. 1995, *ApJ*, 444, 567

- Parmar, A. N., et al. 1997, A&AS, 122, 309
- Pesce, J. E., et al. 1997, ApJ, 486, 770
- Pian, E., et al. 1997, ApJ, 486, 784
- Pian, E., et al. 1998, ApJ, 492, L17
- Sreekumar, P. & Vestrand, W. T. 1997, IAU Circ., 6774, 2
- Stecker, F. W. & De Jager, O. C. 1998, A&A, 334, L85
- Takahashi, T., et al. 1996, ApJ, 470, L89
- Tavecchio, F. , Maraschi, L. & Ghisellini, G. 1998, ApJ, 509, 608
- Treves, A., et al., 1998, Proc. of the BL Lac Phenomenon meeting, Turku, Finland, 22-26
June 1998, Edited by L.O.Takalo, PASP Conf. Series in the press.
- Ulrich, M.-H., Maraschi, L., & Urry, C.M. 1997, ARA&A, 35, 445
- Urry, C. M. & Padovani, P. 1995, PASP, 107, 803
- Urry, C. M., et al. 1993, ApJ, 411, 614
- Urry, C. M., et al. 1997, ApJ, 486, 799
- Vestrand, W. T., Stacy, J. G., & Sreekumar, P. 1995, ApJ, 454, L93
- Zhang, Y.H., et al. 1999, ApJ, to be submitted

Fig. 1.— MECS light curve at 120 s resolution. As described in the text, the spectral analysis has also been performed in separate time intervals, indicated as A to F in the figure.

Fig. 2.— Light curves and Hardness Ratios for different energy bands, in 1000 s bins. In the top three panels we show the light curves in the 0.1-1 keV, 2-4 keV and 4-10 keV energy bands, respectively, while the bottom two panels show the 2-4/0.1-2 and 4-10/2-4 ratios. Note that the coverage of the LECS is more limited than the one of the MECS, because the LECS is operated only during dark times, in order to avoid UV light contamination through the entrance window. The points simultaneous with the presence of LECS data are indicated as bold diamonds. The 2-4/0.1-2 Hardness ratio shows a clear correlation with the source intensity.

Fig. 3.— Discrete Correlation Function between the 0.1-1.5 keV and 3.5-10 keV light curves (binned in 300 s intervals, using a DCF bin size of 0.2 hr) together with its gaussian fit. A positive lag indicates that the high energy X-rays lead the low energy ones.

Fig. 4.— MMD for the same light curves and with the same conventions used in Fig. 3, with its own gaussian fit.

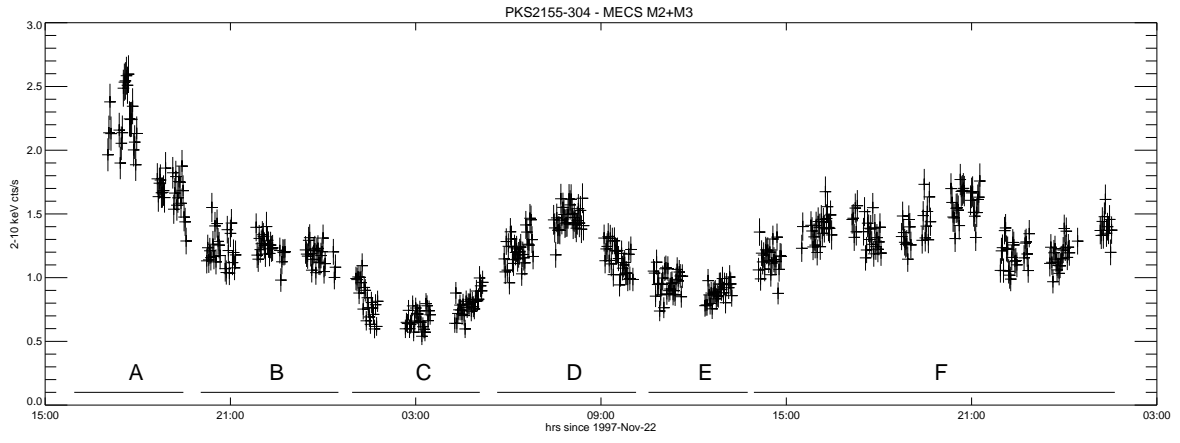
Fig. 5.— LECS+MECS spectra fitted with the broken power law model (see Table 1).

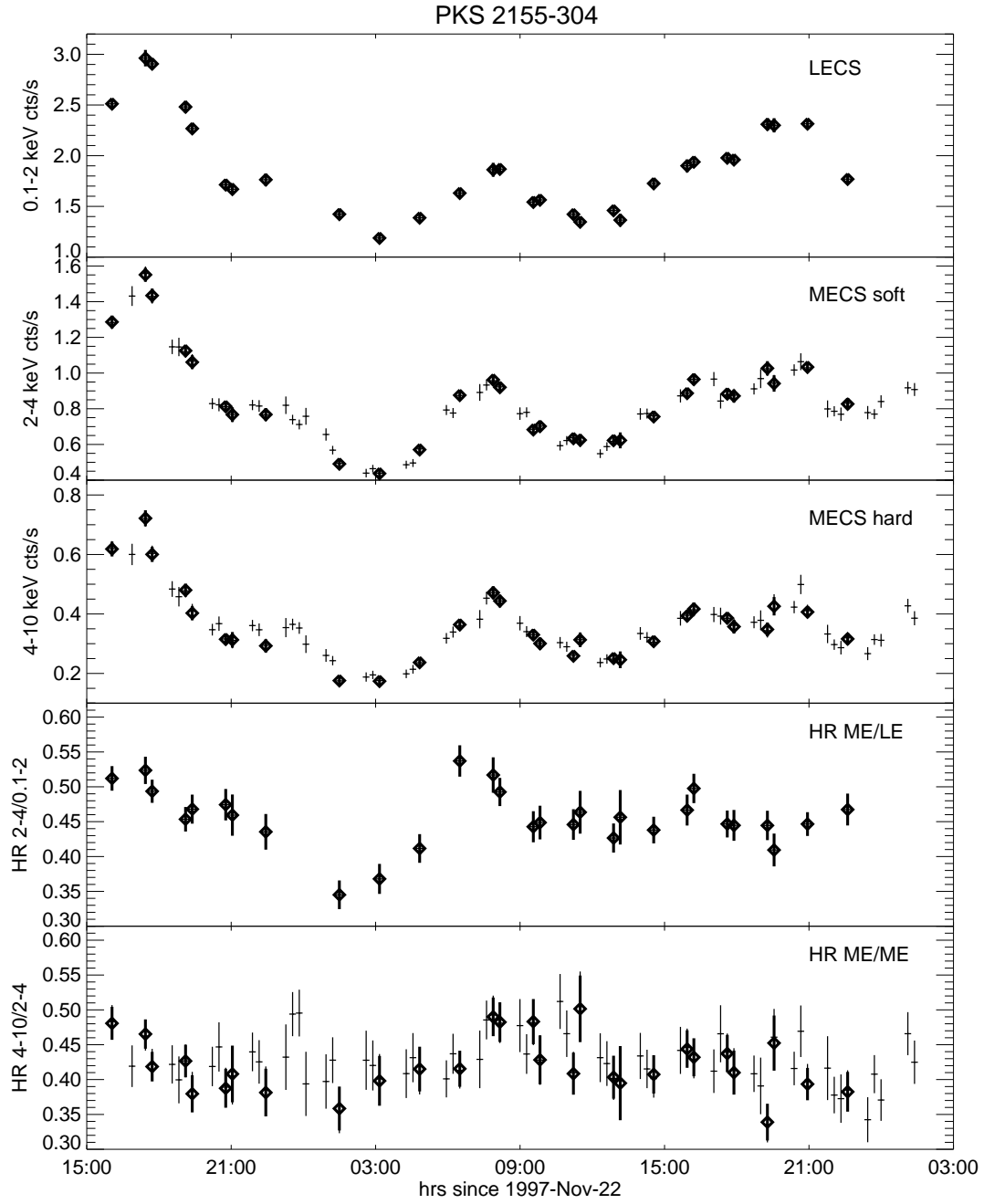
Fig. 6.— MECS+HPGSPC+PDS spectra fitted with a single broken power law. Note the logarithmic scale for the data/fit ratio.

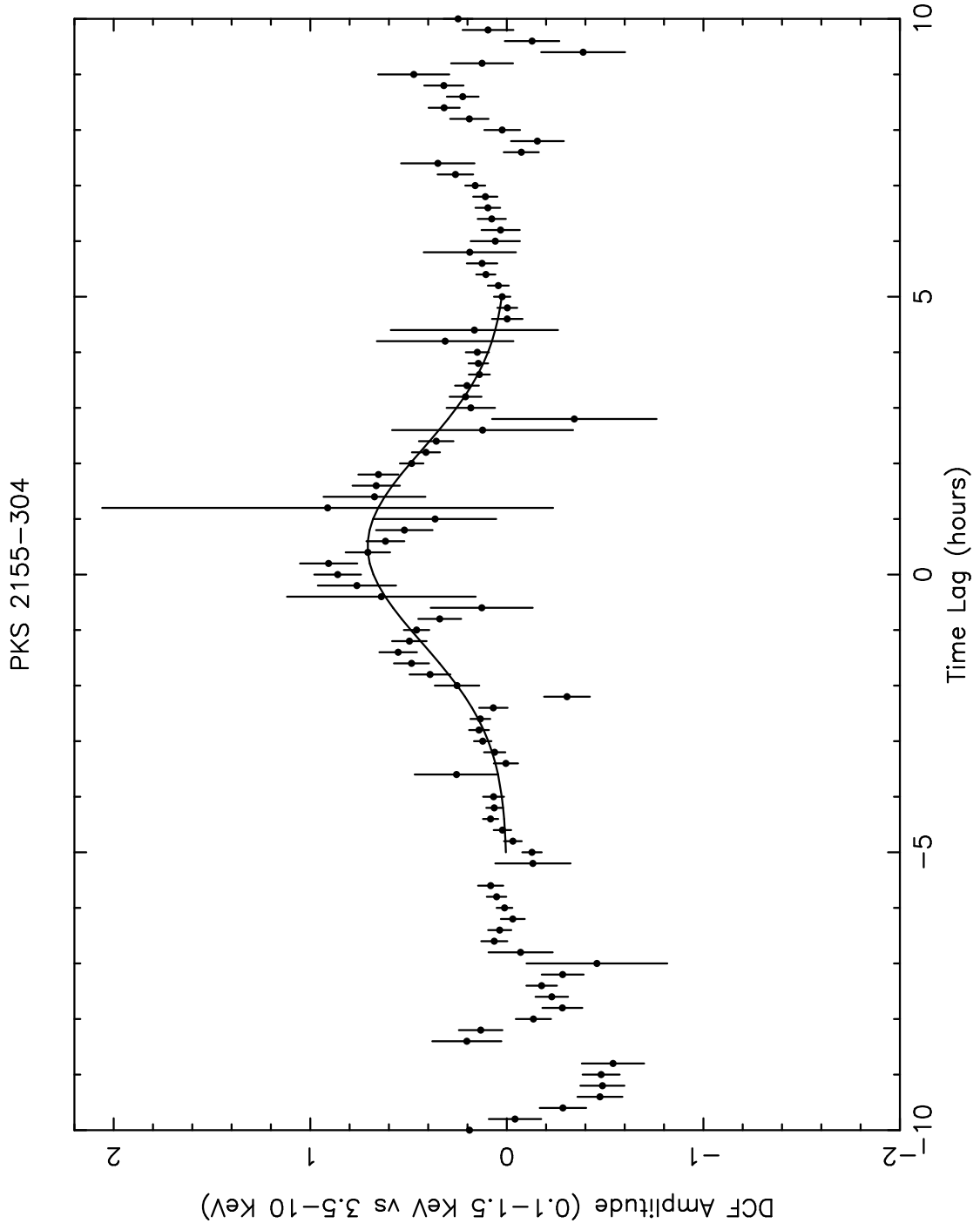
Fig. 7.— Ratio between the flaring state spectrum (A) and the quiescent spectrum (states C and E). The plot shows that the spectrum hardens during the flare but the estimated variation in the spectral index is very small.

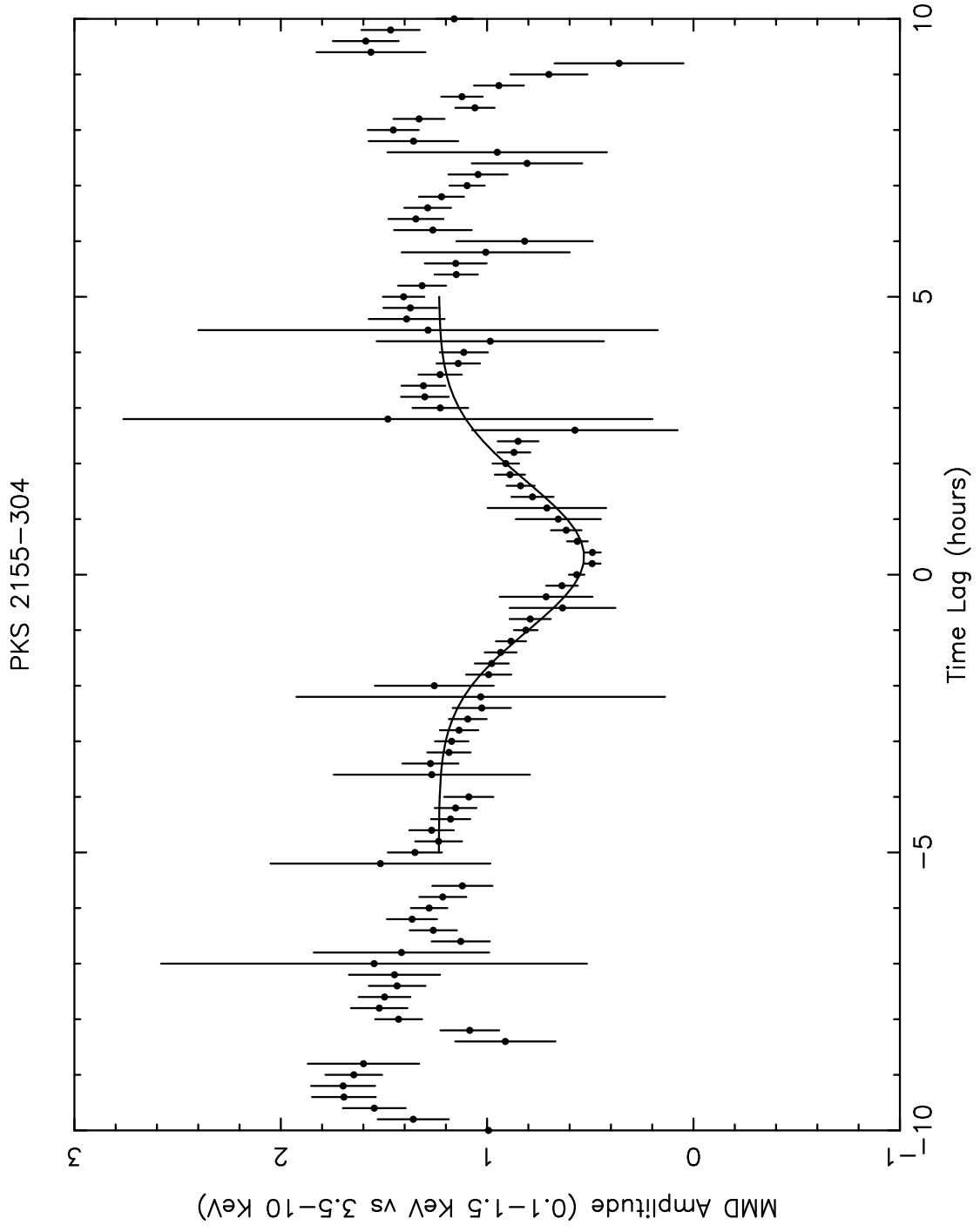
Fig. 8.— The SED of PKS 2155-304 with the fit obtained with the SSC homogeneous model

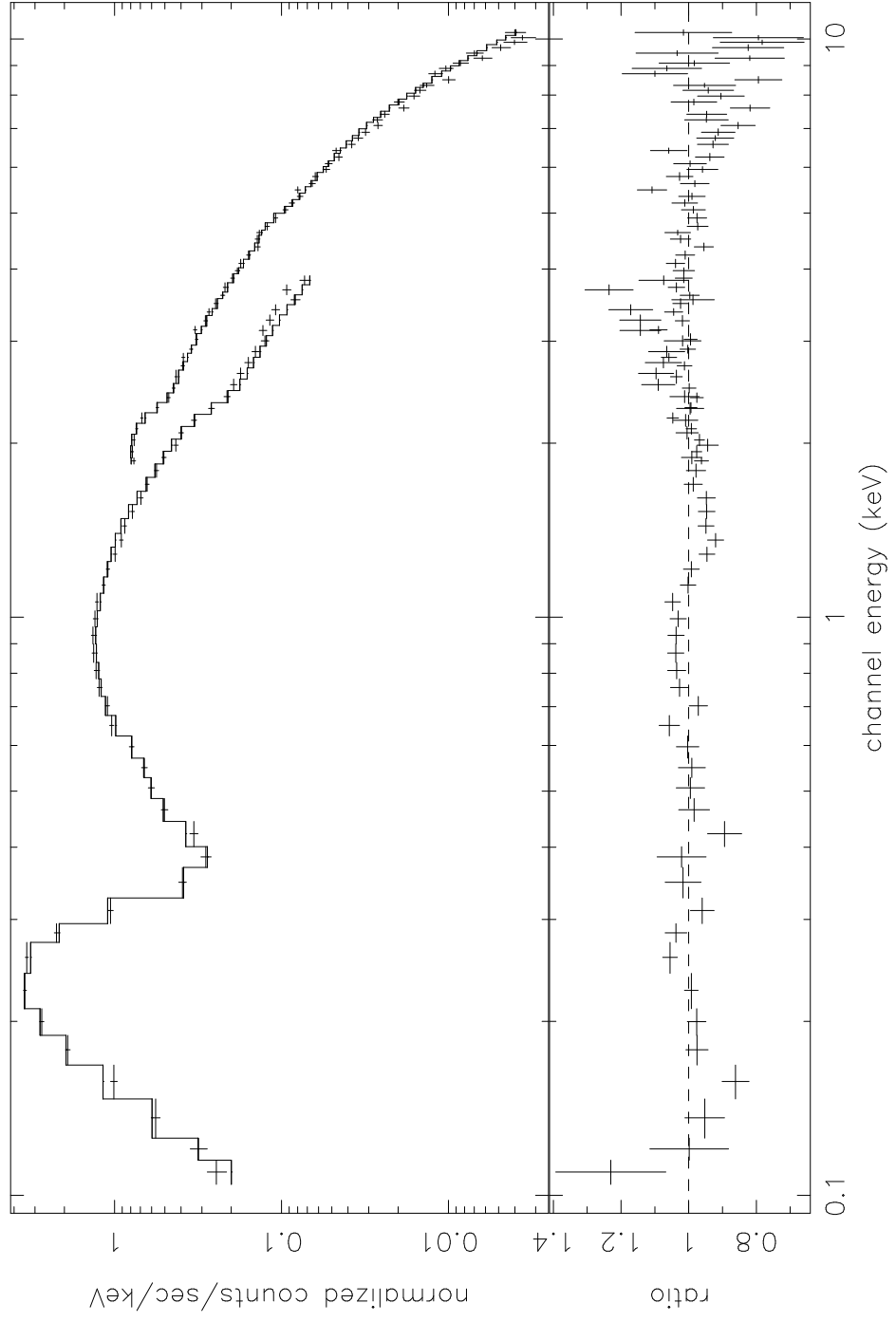
in the high (solid) and low (dashed) states. The parameters of the model are reported in the text. The X-ray points (error bars) represent the spectra in the high (interval A) and low (intervals C+E) states. The thick circles corresponding to the PDS points refer to the average spectrum. The circles are EGRET γ -ray data from Vestrand et al (1995), and they are also shown (as crosses) multiplied by a factor of three to reproduce the gamma-ray state of November 1997. The TeV observation (from Chadwick et al. 1998) is also shown (filled circle). The vertical bars encompass the range between the minimum and maximum value in a compilation of radio, optical and UV data (see text for references).

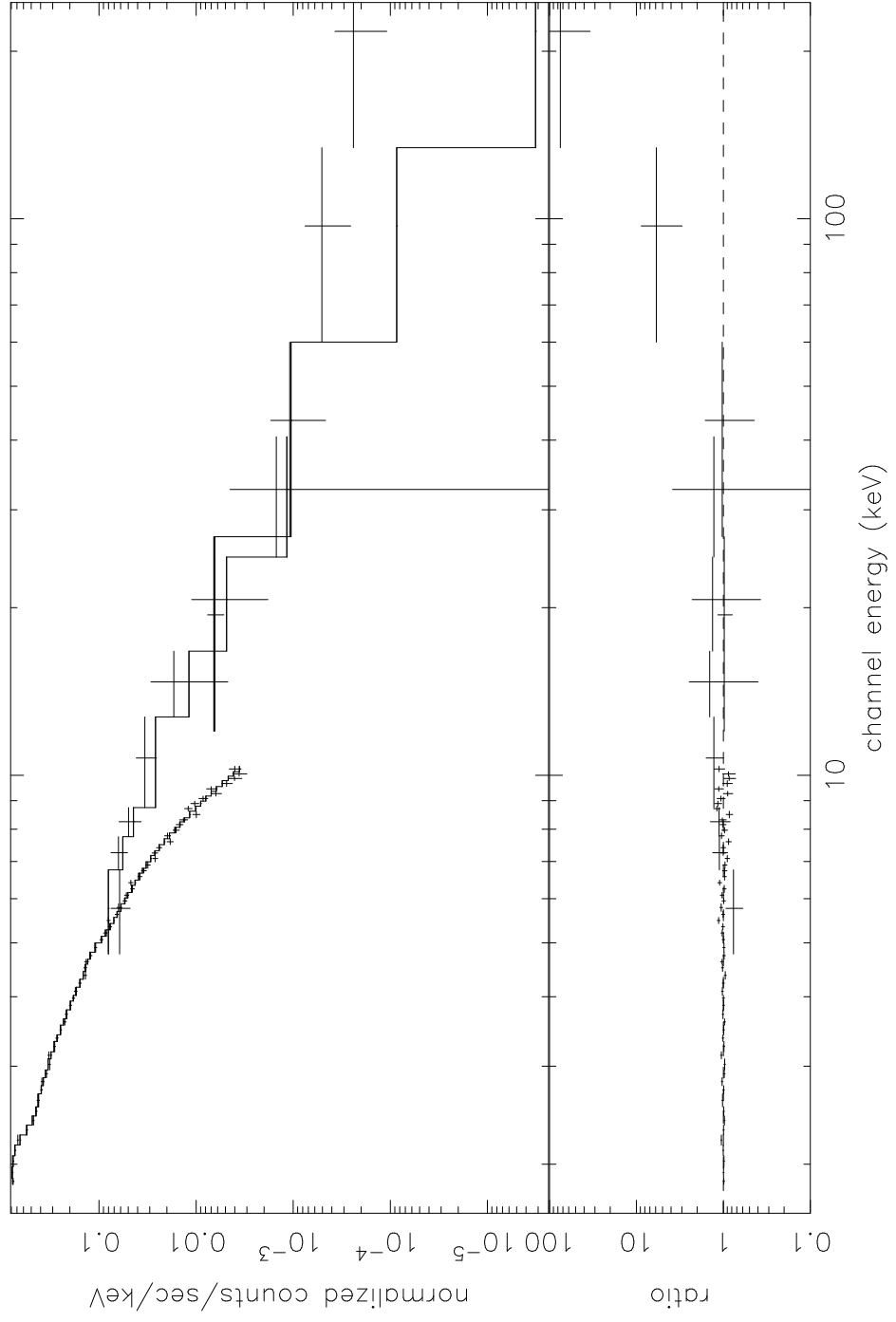


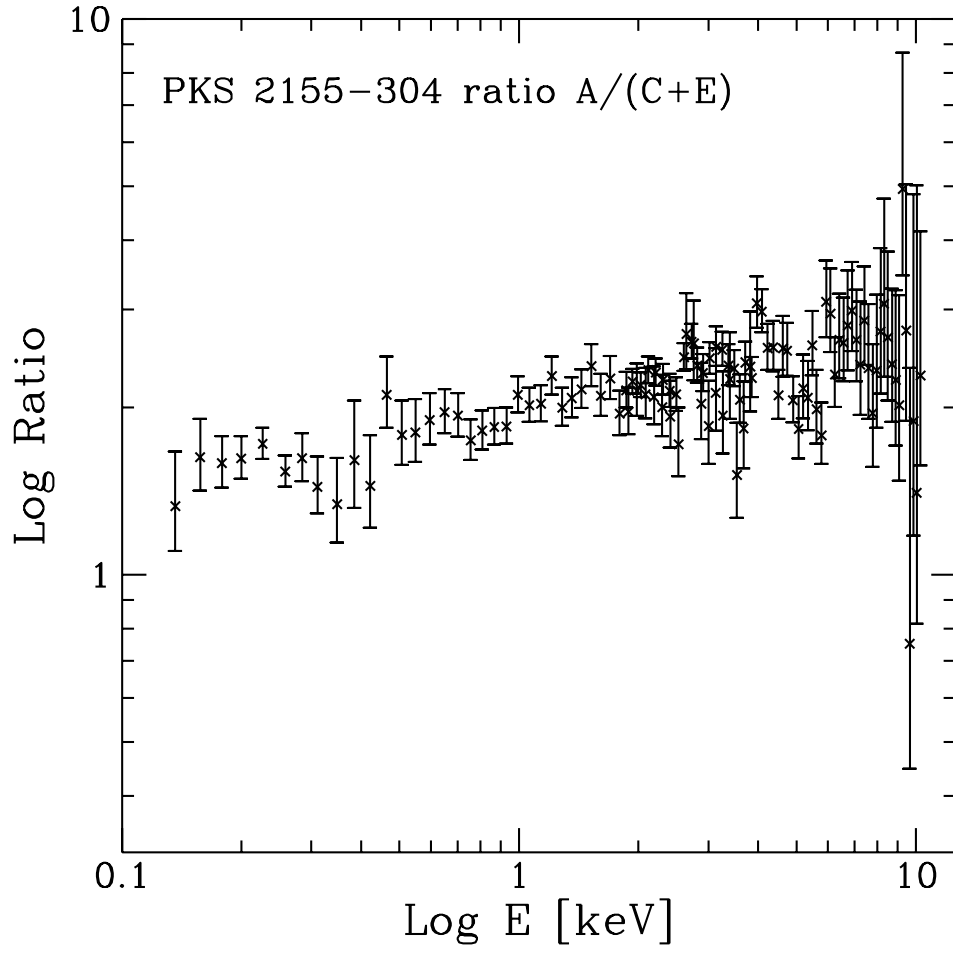












PKS 2155-304

